Ceramics-Silikáty 68 (1), 58-66 (2024)
www.ceramics-silikaty.cz doi: 10.13168/cs.2024.0005

IMPROVING THE STRUCTURAL, DIELECTRIC, AND ELECTRICAL CONDUCTIVITY PROPERTIES OF BISMUTH-DOPED STRONTIUM TITANATE VIA MICROWAVE SYNTHESIS TECHNOLOGY

KHALID ELFAKI IBRAHIM*, #H. A. KASSIM**

*Department of Zoology, College of Science, King Saud University, P.O. Box 2455, Riyadh 11451, Saudi Arabia
**Department of Physics, College of Science, P.O. BOX 2455, King Saud University, Riyadh 11451, Saudi Arabia

#E-mail: hkassim@ksu.edu.sa

Submitted November 16, 2023; accepted December 14, 2023

Keywords: Microwave synthesis, Dielectric constant, AC conductivity, Activation energy

Polycrystalline $Sr_{1-x}Bi_xTiO_3$ (SBTx) ceramics were synthesized by applying microwave heating to the precursor components in a solid-state process. X-ray diffraction studies revealed the formation of a sole perovskite phase (ABO_3), with no evidence of any secondary phase. Scanning electron microscopy facilitated the observation of images that exhibited a substantial, granular morphology. The dielectric properties were investigated at ambient temperature. The dielectric constant rose from 1021 to 2320 with increasing concentrations of Bismuth (Bi), while the dielectric loss experienced an increase from 0.01 to 0.12. The investigation into the alternating current (AC) conductivity revealed a positive correlation between the AC conductivity and the frequency. The electron transport in SBTx ceramics was analyzed based on the measured AC conductivity, concluding that the correlated barrier hopping model provides the most accurate description of the phenomenon. The investigation involved the analysis of the activation energy for conduction in various materials by utilizing Arrhenius plots. The drop in the concentrations of Bi leads to a reduction in the activation energy. The observed reduction in activation energy is hypothesised to be attributed to an appealing interaction between the doped cations and the oxygen vacancies.

INTRODUCTION

The processing of ceramics significantly impacts the quality of the resulting uniform body. The acquisition of its microstructure and ultimate qualities is significant. Advanced ceramics are often processed using high-temperature methods, such as conventional sintering and mould casting. Manufacturing ceramics at high temperatures necessitates significant financial investment and substantial energy use. As a result, novel technologies, such as microwave processing, are being offered as non-conventional sintering methods to address the issues of cost and energy consumption while enhancing the qualities of the ceramic materials produced. In microwave heat treatment, the materials are subjected to microwave radiation, which is absorbed and converted into thermal energy [1-5]. Microwave processing has been found to offer numerous advantages over conventional processing techniques. These include enhanced diffusion processes, reduced energy consumption, a decreased processing time, a lower sintering temperature, and improved physical properties [6-9]. Various techniques have been employed in fabricating $SrTiO_3$ ceramic materials, including solid-state reaction [10] and sol-gel methods [11]. These approaches have specific concerns, including extended time requirements, elevated energy usage, and the need for phase purity, one potential approach to improving the dielectric permittivity for enhancing the energy storage performance of $SrTiO_3$ ceramics. The modification of dielectric characteristics in $SrTiO_3$ can be accomplished by introducing impurities into the host material [12]. Introducing donor ions into polycrystalline strontium titanate manifests in intriguing and valuable dielectric characteristics [13]. The dielectric constant of $SrTiO_3$ ceramics can be enhanced by doping with cations possessing larger or smaller ionic radii, such as Ba^{2+} [14], Mn^{2+} [15], and trivalent rare earth ions [RE^{3+}] [16, 17]. The dipole moment reorientation significantly impacts the physical characteristics of strontium titanate. In instances of this nature, the dissimilarity in the ionic radius between dopants and host compounds can simultaneously result in off-center dipole moments [18]. Strontium titanate ($SrTiO_3$) is a significant illustration of a perovskite compound that exhibits diverse

chemical defects, which can notably impact its conductivity [19]. The impact of chemical defects on the conductivity in doped $SiTiO_3$ with donor ions [20-22] is extensively documented in the literature. The conductivity enhancement in ceramics based on $SrTiO_3$ can be achieved by strontium on the A-site of the perovskite structure with cations such as bismuth (Bi). In this investigation, microwave irradiation was employed to facilitate the heating process of the initial substances, resulting in a reduced time and energy usage. This approach holds promise for the industry as a sustainable strategy in the forthcoming years. The present study aimed to evaluate the impact of microwave synthesis on the crystal structures, microstructures, dielectric, and conductivity of Bi-doped $SrTiO_3$. The results obtained in this study demonstrate that microwave synthesis is an effective method for achieving the necessary microstructure with a single phase.

EXPERIMENTAL

The solid solution was synthesised by using the initial substances of strontium carbonate ($SrCO_3$), bismuth oxide (Bi_2O_3) with a purity of 99.99 % from Sigma-Aldrich, and titanium dioxide (TiO_2) with a purity of 99.98 % from Sigma-Aldrich. The mixture was subjected to milling in an agate mortar while acetone was added for a length of 10 hours. Subsequently, the mixture was subjected to calcination using a Microwave Sintering System (MWSS) for 15 minutes. The experimental conditions included maintaining a target temperature of 1000 °C while using a heating and cooling rate of 50 °C per minute. The powders were compressed into disc-shaped pellets by using a binder consisting of 1 wt. % Poly Vinyl Alcohol (PVA). The process of binder evaporation included heating the green pellets to a temperature of 500 °C, with a heating rate of 2 °C per minute. The sintering process was conducted using a Microwave Sintering System (MWSS), with a temperature of 1200 °C for 30 minutes. Four distinct compositions were generated by manipulating the quantities of Bi at the Sr site in $SrTiO_3$, with the respective values of x being 0, 0.02, 0.04, and 0.08. The structural analysis of all the specimens was conducted at ambient temperature using a Bruker D8 powder X-ray diffractometer equipped with Cu-Kα radiation, covering a 2θ range spanning from 20° to 70° with the assistance of FullProf refinement. The phase confirmation was performed using a FullProf refinement program. The Scherrer formula determines the samples' crystallite size (D_P). The morphological structure of the sintered samples was examined using a field emission scanning electron microscope (FE-SEM) (JSM7600F). The transmission electron microscopy (TEM) images were taken using JEM-2100F to investigate the ceramic SBT0.08 d_{110}-spacing using the selective area electron diffraction (SEAD) analysis. The relationship between the permittivity and the frequency was examined from 1 kHz to 2 MHz at room temperature using an Agilent E4294A impedance analyzer. The AC electrical conductivity of all the samples was determined using the complex dielectric constant's real and imaginary components. The activation energy was estimated using Arrhenius plots to analyze the temperature dependence of the AC conductivity in the pure $SrTiO_3$ ceramics and $SrTiO_3$ ceramics doped with Bi.

RESULTS AND DISCUSSION

Figure 1a illustrates the X-ray diffraction patterns obtained from the fabricated SBTx ceramics. The samples under observation have a singular cubic structure characterised by the space group Pm3m (JCPDS Card No. 35-0734) [23]. There is no discernible second phase seen. Incorporating Bi^{3+} ions into the Sr^{2+} lattice leads to

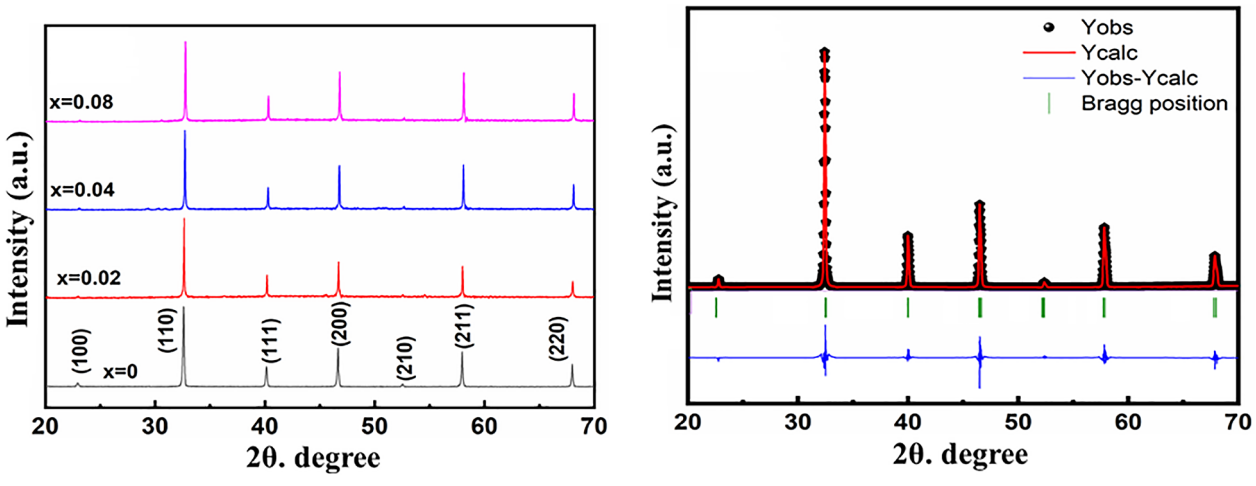

a) b)

Figure 1. X-ray diffraction patterns (a), FullProf refinement for the sample with x = 0.08 (b). *(Continue on next page)*

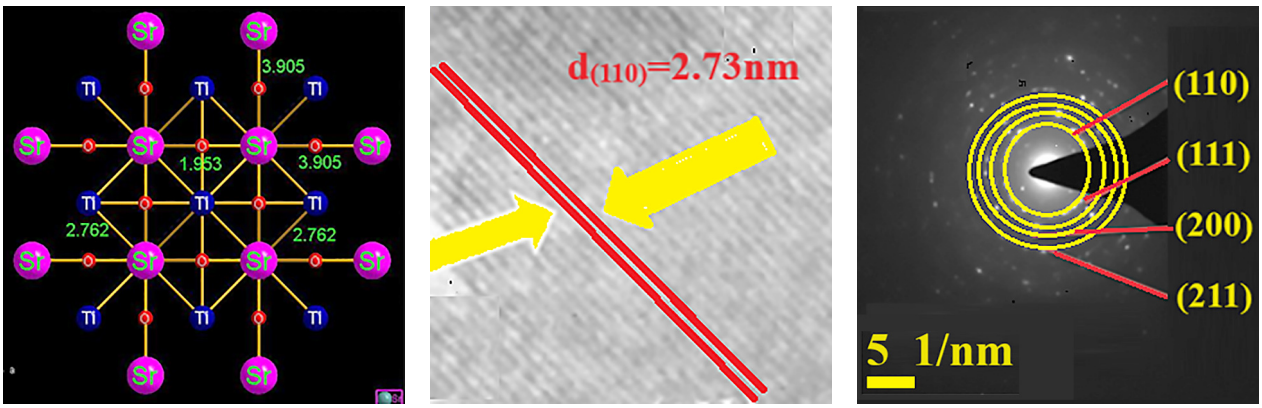

c) d) e)

Figure 1. Schematic diagram for the crystal structure of $SrTiO_3$ designed by using VESTA software (c), high-resolution scanning transmission electron microscopy (HR-TEM) image shows the d-spacing (d) and the selected area electron diffraction (SAED) for the sample with $x = 0.08$ (d).

the marginal displacement of the peaks towards higher 2θ values, as seen in the graph on the right side of Figure 1a. The observed shift demonstrates a reduction in the lattice parameter and unit cell volume, as seen in Table 1. The observed variance may be elucidated upon by examining the doping of Sr^{2+} ions with Bi^{3+} ions, the latter having a lower ionic radius. The ionic radii of Bi^{3+} (IR = 1.03 Å) are smaller than that of Sr^{2+} (1.44 Å) [24], which results in a noticeable shift in the peaks towards higher 2θ angles. This shift leads to a decrease in the lattice parameter. A decreased lattice parameter (a) when doping involves substituting a sizeable ionic radius with a smaller one has previously been reported in the literature [25]. The refinement analysis shown in Figure 1b is performed to substantiate the findings above. The unit cell's volume decreased when the amount of Bi^{3+} increased. This may influence the observed reduction in the unit cell, resulting in a reduction in the unit cell volume of the ST crystal. Moreover, the phenomenon of peak widening exhibits an augmented trend as the doping concentration increases, suggesting a concomitant reduction in the size of crystallites. The crystallite size of the investigated samples was calculated using the formula reported in Reference [26]:

$$D_p = \frac{K\lambda}{\beta \cos\theta} \quad (1)$$

Table 1. The lattice parameter, unit cell volume, crystallite size of the sintered SBTx ceramics estimated from refinement.

Bi content	Lattice constant (Å)	Unit cell volume $(Å)^3$	D_p (nm)
0	3.9091	59.73	61
0.02	3.9072	59.64	58
0.04	3.9067	59.63	55
0.08	3.9053	59.65	51

The investigation of the $x = 0.08$ sample included examining its d_{hkl} spacing using high-resolution transmission electron microscopy (HR-TEM), and it was found to be equal to 2.73 nm, as seen in Figure 1d. The superimposition of bright spots with a Debye ring pattern in Figure 1d of the selected area electron diffraction (SAED) patterns suggests that the materials under investigation possess a polycrystalline structure, as previously reported, which is consistent with the results obtained from X-ray diffraction (XRD) analysis.

Figure 2 displays the scanning electron microscopy (SEM) images of the sintered SBTx ceramics, where x values of 0, 0.02, 0.04, and 0.08 were used. The photos show that all the samples exhibited thick structures with varying grain sizes and shapes. In general, the grain size of the pure sample is more significant than that of the doped samples. Precisely, the average grain size for pure $SrTiO_3$ is 1.5 μm. However, this value decreases as the concentration of Bi increases, reaching a minimum value of approximately 0.66 μm for the sample with $x = 0.08$, as depicted in Figure 2. The reduction in grain size may be explained as follows: Both bismuths serve as donor dopants in the Sr-site of the ST host lattice. The presence of an excessive number of donors results in the generation of voids within the strontium material [27]. Therefore, strontium vacancies are a crucial contributing element to the observed enhancements in the density and the formation of small grain sizes in the samples. On the other hand, the microwave sintering process can play a significant role in reducing the grain size [28-30]. The impact of microwave sintering on the expansion of the grain size is intricate and contingent upon many aspects, including the composition of the material undergoing sintering, the parameters used throughout the sintering process, and the existence of additives or subsequent phases. Nevertheless, it is well observed that microwave sintering can mitigate grain development compared to traditional sintering methods.

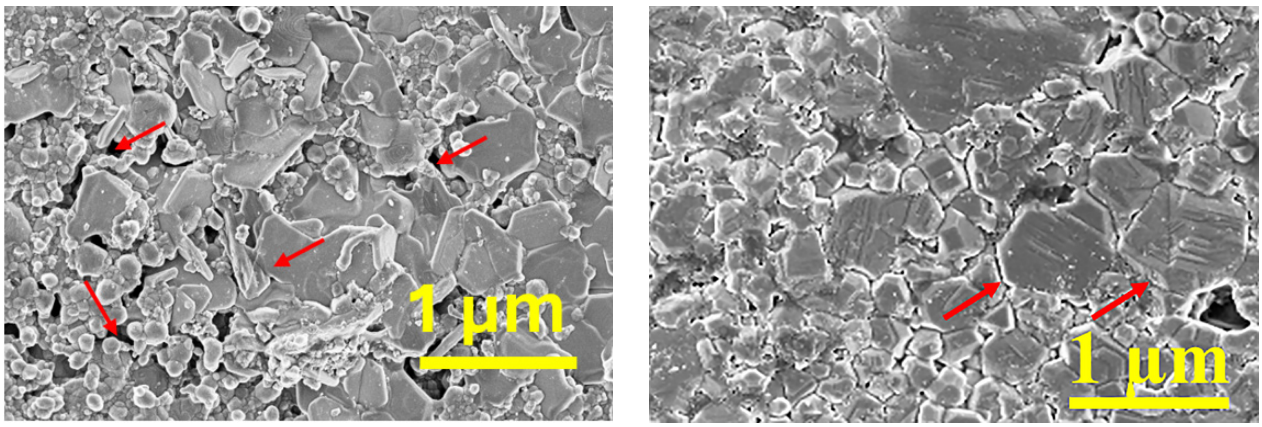

a) $x = 0$ b) $x = 0.02$

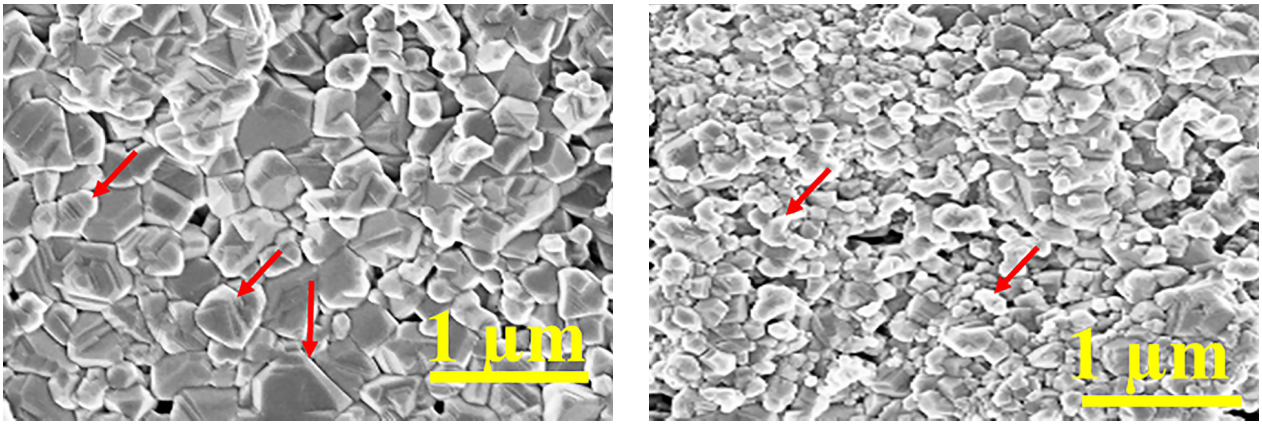

c) $x = 0.04$ d) $x = 0.08$

Figure 2. SEM images of the Microwave sintered SBTx ceramics with: a) $x = 0$, b) $x = 0.02$, c) $x = 0.04$, and d) $x = 0.08$.

The phenomenon described may be due to the uniform heating and quick densification produced by microwave sintering. This process effectively lowers the available time for grain growth to take place. Numerous theories have been postulated to explain the phenomenon of grain growth inhibition seen during microwave sintering [31, 32]. The mobility of grain boundaries may be diminished by the high heating and cooling rates characteristic of microwave sintering, hence impeding the process of grain development. This reduction in porosity restricts the available area for grain development inside the material.

Dielectric property measurements and analytical methods may be used to investigate the permittivity characteristics as a function of frequency. Two essential properties of these materials are evaluated:

- their ability to retain an electric charge (capacitive property),
- their ability to transport an electric charge (conductive property).

The material's dielectric constant and loss tangent may be determined using this research. The frequency evolution of the dielectric constant and dielectric loss for sintered ceramics at room temperature is shown in Figure 3a. According to the data provided in the graph, the dielectric constant decreases as frequency rises. The phenomena of a decreasing dielectric constant as the frequency increases may be explained by conside-

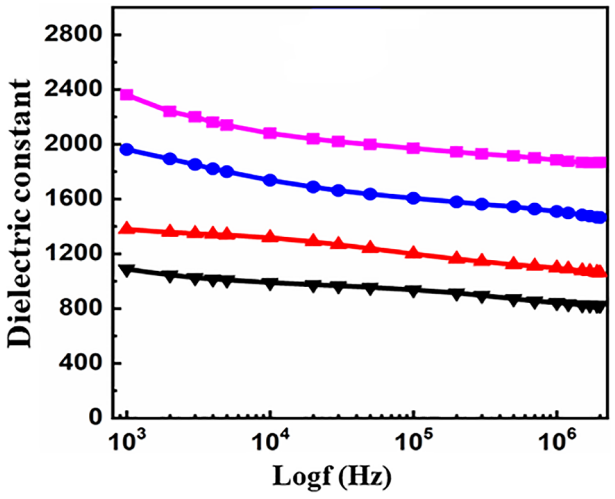

a)

Figure 3. Variations in the: a) dielectric constant. *(Continue on next page)*

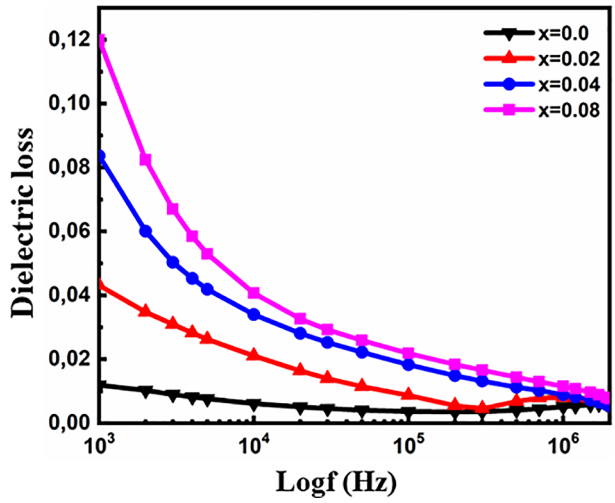

b)

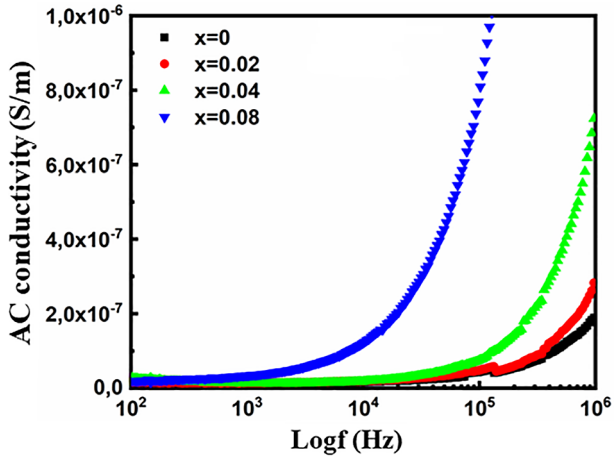

c)

Figure 3. Variations in the: b) the loss tangent (tan δ) with logf (Hz) at room temperature temperatures for sintered ceramics; c) the frequency dependence of the AC conductivity measured at room temperature.

ring the effect of different polarisabilities, such as deformation (ionic and electronic) and relaxation (interfacial and orientation) polarization [34-36]. The sum of these four polarization categories is the dielectric material's overall polarization [36]. The phenomenon of orientation polarization decreases in cases of increased frequency owing to the longer length necessary for flip-flopping in contrast to electronic and ionic polarization. This phenomenon lowered the dielectric constant until it reached a stable value at higher frequencies. Furthermore, it is clear from the study in Figure 3a that the dielectric constant rises as the Bi concentration increases. The observed increase in the dielectric constant might be explained by the orientation polarization caused by the movement of molecules or dipoles. As a result, dipoles reorient themselves more efficiently when the concentration of bismuth (Bi) is more significant. The change in dielectric loss with the frequency for the sintered SBT*x* ceramics at room temperature is seen in Figure 3b. The graph shows a positive relationship between the dielectric loss and Bi concentration. The existing literature divides the dielectric loss into conduction, dipole, and vibration losses [37]. Conduction loss is the process by which ions travel over long distances. The energy dissipation in the lattice is caused by ion mobility, and the dissipation per cycle is proportional to the conductivity [38]. Lower and intermediate frequency areas have more considerable dielectric losses due to the combination of ion jump and conduction loss via ion migration and ionic polarisation [39]. At higher frequencies, the vibrations of ions may be the sole source of the loss tangent, resulting in a reduction in dielectric loss. AC conductivity is an excellent way to learn about the nature of ionic motion in ionically conducting materials.

At room temperature, the change in the AC conductivity with the frequency in the 1 kHz –1 MHz range for sintered ceramics was examined. Figure 3c depicts the experimental findings as a function of frequency. The rise in the alternating current (AC) conductivity with the frequency is the typical behaviour found in some materials, and it is often connected with the material's reaction to the applied electric field at various frequencies [40]. This phenomenon is significant in the research of electrical characteristics of materials, such as dielectric spectroscopy. Response to an applied electric field in materials having polarisation processes, such as Bi-doped ST ceramics in Figure 3c, might entail reorienting or moving charged particles (e.g., electrons or ions) inside the material. These particles may need more time to adequately react to the fast-changing electric field at lower frequencies, resulting in poorer AC conductivity. The particles inside the material have more opportunity to respond to the changing electric field as the frequency rises. The conductivity hits a plateau or increases with the frequency at some point, suggesting that the material becomes more conductive at higher frequencies. This behaviour is often related to Maxwell-Wagner polarisation in heterogeneous materials or charge carrier dynamics in conductive materials [41]. The mechanics might differ based on the substance and frequency range of interest.

Figure 4 displays the Arrhenius plots illustrating the temperature dependence of the AC conductivity for SBT*x* ceramics. The estimation of a material's activation energy may be derived by analyzing the temperature dependency of its AC (alternating current) conductivity using the Arrhenius equation. The Arrhenius equation establishes a connection between the temperature dependency of a reaction rate or, in this context, the conductivity, the activation energy (E_a), and other relevant variables. The Arrhenius equation is expressed as follows [42]:

$$\sigma(T) = \sigma_0 \cdot e^{-E_a/kT} \quad (2)$$

where symbol $\sigma(T)$ represents the conductivity at a specific temperature T. The term σ_0 refers to the pre-ex-

ponential factor or pre-exponential conductivity. E_a represents the activation energy. The symbol k denotes the Boltzmann constant. Lastly, T represents the absolute temperature measured in Kelvin. Conducting AC conductivity experiments at various temperatures is customary to determine the activation energy from experimental AC conductivity data. Next, create a graph by plotting the natural logarithm of $\sigma(T)$ against the reciprocal of $1/T$. Subsequently, use a linear regression analysis to determine the best-fit line for the data. The slope of the line is associated with the product of the Boltzmann constant (k) and the activation energy (E_a). By analysing the data, the activation energy values were determined to be 0.22 eV, 0.13 eV, 0.084 eV, and 0.05 eV. The obtained data indicate a reduction in the activation energy as the concentration of Bi increases. The drop in activation energy may be attributed to the attractive interaction between the substituted cations and the oxygen vacancies [43-45]. Bismuth ions are present at the strontium (Sr^{2+}) site, creating defects to achieve charge neutralisation. The primary mobile charges contributing to polarisation, conduction, and activation energy are attributed to the defects, namely the bismuth and oxygen vacancies. The observed reduction in the activation energy suggests the occurrence of defect coupling, which hinders the migration of oxygen vacancies and, therefore, limits the enhancement in the conductivity [46]. Perovskite ferroelectric materials have been shown to have comparable behaviour in the literature [47]. The activation energy denotes the energy necessary for transporting the charge carriers, such as electrons, ions, or both, inside the crystal lattice or defect sites [48, 49]. The processes responsible for conductivity in ceramics exhibit significant variation, contingent upon the exact kind of ceramics and their composition. The phenomenon of ionic conductivity may be seen in some ceramics, whereby the movement of ions inside the material facilitates the conduction process [50]. Conversely, electronic conductivity can be observed in other ceramics, where the conduction is reduced by the movement of electrons across the crystal lattice.

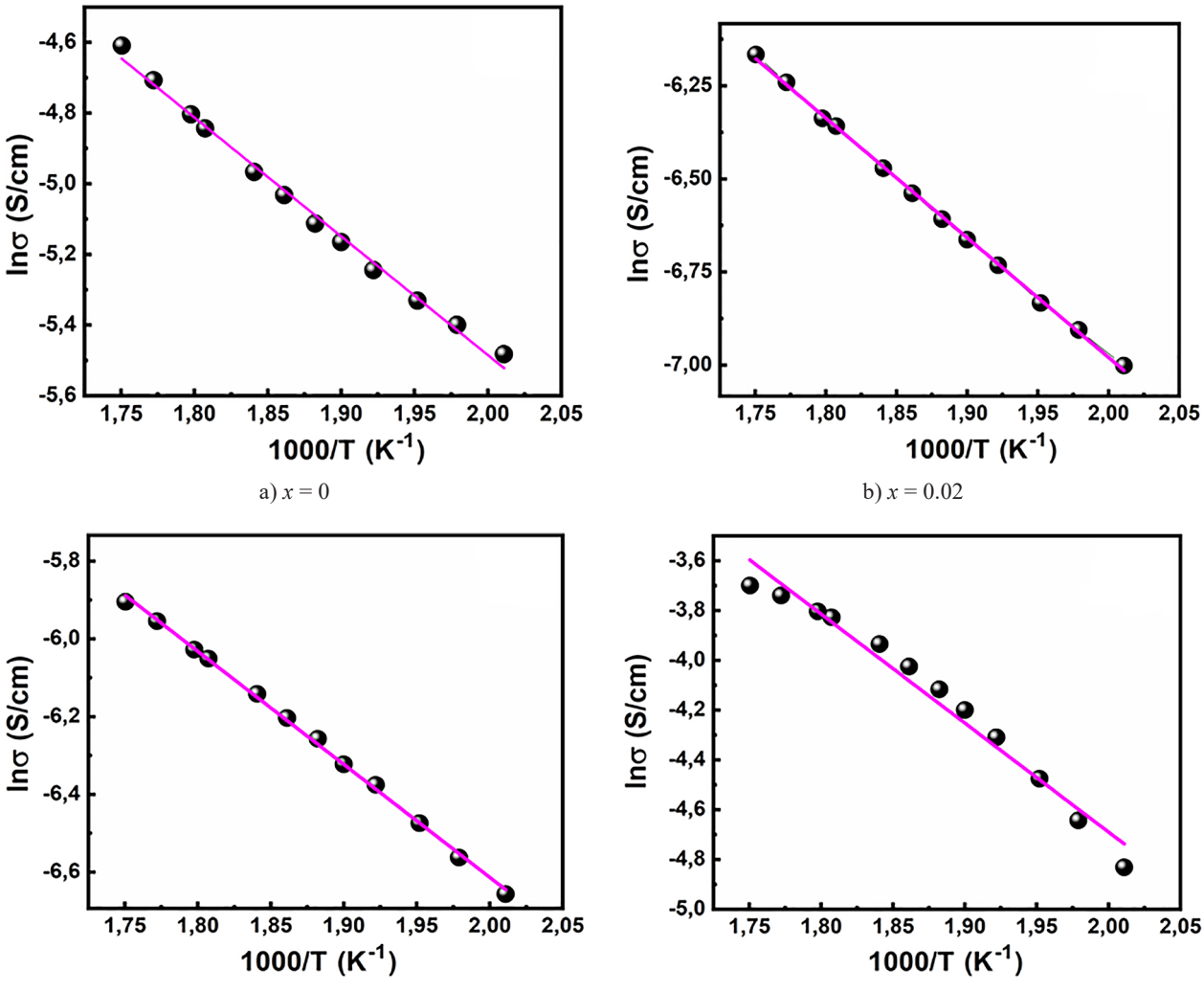

a) $x = 0$ b) $x = 0.02$

c) $x = 0.04$ d) $x = 0.08$

Figure 4. Arrhenius plots of the temperature dependence of the AC conductivity of the SBTx ceramics with: a) $x = 0$, b) $x = 0.02$, c) $x = 0.04$, and d) $x = 0.08$.

CONCLUSION

Polycrystalline $Sr_{1-x}Bi_xTiO_3$ (SBT*x*) ceramics were synthesised using microwave heating to the precursor components in a solid-state method. X-ray diffraction techniques provided insights into the production of a singular perovskite phase (ABO_3) without any discernible presence of any further secondary phases. Scanning electron microscopy enabled one to visually examine pictures that display a significant, granular structure. The investigation focused on the dielectric characteristics at ambient temperature across several frequencies. The dielectric constant increases from 1025 to 2320 as the Bismuth (Bi) concentrations increased. Examining the alternating current (AC) conductivity showed a direct relationship between the AC conductivity and the frequency, when investigating the electron transport in SBTx ceramics by analysing the AC conductivity measurements. The study's findings suggest that the correlated barrier hopping model offers the most precise explanation for this phenomenon. The study used Arrhenius plots to examine the activation energy associated with the conduction in different materials. An increase in bismuth (Bi) concentrations results in a corresponding decrease in the activation energy. The decreased activation energy is postulated to result from the attractive interaction between the doped cations and the oxygen vacancies.

Acknowledgement

The author thanks the Researchers Supporting Project (RSPD2024R759), King Saud University, Riyadh, Saudi Arabia, for the financial support.

REFERENCES

1. Sikder P., Ren Y., Bhaduri S. B. (2020): Microwave processing of calcium phosphate and magnesium phosphate-based orthopaedic bioceramics: A state-of-the-art review. *Acta Biomaterialia, 111*, 29-53. doi: 10.1016/j.actbio.2020.05.018
2. Szafraniak B., Fusnik Ł., Xu J., Gao F., Brudnik A., Rydosz A. (2021): Semiconducting Metal Oxides: $SrTiO_3$, $BaTiO_3$ and $BaSrTiO_3$ in Gas-Sensing Applications: A Review, *Coatings, 11*, 185. doi: 10.3390/coatings11020185
3. Alkathy M. S., Pattipaka S., Gatasheh M. K., Kassim H. A., Saad Daoud M., Eiras J. A. (2023): Achieving high energy storage performance and efficiency in lead-free $SrTiO_3$ ceramics via neodymium and lithium co-doping technique. *Journal of Asian Ceramic Societies*, *11*(4), 491-503. doi: 10.1080/21870764.2023.2259149
4. Alkathy M. S., Ali S. M., Goud J. P., Mastelaro V. R., Zabotto F. L., Milton F. P., et al. (2023): Achieving dense microstructure with desired physical properties rapidly and inexpensively in Bi-modified $SrTiO_3$ ceramics via microwave sintering technique. *Journal of Materials Science: Materials in Electronics, 34*(22), 1616. doi: 10.1007/s10854-023-11034-0
5. Alkathy M. S., Raju K. J. (2019): Microwave-Assisted Synthesis and Characterization of Strontium Titanate Nanoparticles. *Albaydha University Journal, 1*(2), 235-240. doi: 10.56807/buj.v1i2.26
6. Alem S. A. A., Latifi R., Angizi S., Hassanaghaei F., Aghaahmadi M., Ghasali E., Rajabi M. (2020). Microwave sintering of ceramic reinforced metal matrix composites and their properties: a review. *Materials and Manufacturing Processes, 35*(3), 303-327. doi: 10.1080/10426914.2020.1718698
7. Loharkar P. K., Ingle A., Jhavar S. (2019): Parametric review of microwave-based materials processing and its applications. *Journal of Materials Research and Technology, 8*(3), 3306-3326. doi: 10.1016/j.jmrt.2019.04.004
8. Li B., Tang B., Zhang S., Jiang H., (2011): Low-temperature sintered $(ZnMg)_2SiO_4$ microwave ceramics with TiO_2 addition and calcium borosilicate glass. *Ceramics-Silikáty, 55*(1), 14–19.
9. Muthuchamy A., Nagaraju N., Annamalai A. R., Agrawal D. K. (2019): Nd_2O_3 doped yttria-stabilized zirconia ceramics fabricated by conventional and microwave sintering methods. *Ceramics–Silikáty, 63*(1), 45-50. doi: 10.13168/cs.2018.0044
10. Alkathy M. S., Goud J. P., Raju K. J. (2016): Effect of sintering temperature on structural and dielectric properties of Bi and Li co-substituted $SrTiO_3$. In AIP Conference Proceedings (Vol. 1728, No. 1, p. 020355). AIP Publishing LLC. doi: 10.1063/1.4946406
11. Klaytae T., Panthong P., Thountom S. (2013): Preparation of nanocrystalline $SrTiO_3$ powder by sol-gel combustion method. *Ceramics International, 39*, S405-S408. doi: 10.1016/j.ceramint.2012.10.103
12. Pan W., Cao M., Hao H., Yao Z., Yu Z., Liu H. (2020): Defect engineering toward the structures and dielectric behaviors of (Nb, Zn) co-doped $SrTiO_3$ ceramics. *Journal of the European Ceramic Society, 40*(1), 49-55. doi: 10.1016/j.jeurceramsoc.2019.09.027
13. Ouyang T., Pu Y., Li X., Ji J., Zhou S., He C., Wang B. (2022): Influence of current density on microstructure and dielectric properties during the flash sintering of strontium titanate ceramics. *Journal of Alloys and Compounds, 903*, 163843. doi: 10.1016/j.jallcom.2022.163843
14. Alkathy M. S., Raju K. J., Eiras J. A. (2021): Colossal dielectric permittivity and high energy storage efficiency in barium strontium titanate ceramics co-doped with bismuth and lithium. *Journal of Physics D: Applied Physics, 54*(12), 125501. doi: 10.1088/1361-6463/abd12b
15. Diao C., Li H., Yang Y., Hao H., Yao Z., Liu H. (2019): Significantly improved energy storage properties of sol-gel derived Mn-modified $SrTiO_3$ thin films. *Ceramics International, 45*(9), 11784-11791. doi: 10.1016/j.ceramint.2019.03.056
16. Qiao Y., Li, W., Zhang Y., Jing L., Gao C., Cao W., et al. (2020): Hole-pinned defect-dipoles induced colossal permittivity in Bi-doped $SrTiO_3$ ceramics with Sr deficiency. *Journal of Materials Science & Technology, 44*, 54-61. doi: 10.1016/j.jmst.2019.11.012
17. Pradhan J., Mallick H. K., Sahoo M. P. K., Pattanaik A. K. (2021): Enhanced optical and dielectric properties of rare-earth co-doped $SrTiO_3$ ceramics. Journal of Materials Science: *Materials in Electronics, 32*(10), 13837-13849. doi: 10.1007/s10854-021-05959-7

18. Ponnusamy R., Venkatesan R., KaniAmuthan B., Shalini K., Karuppannan A., Murugan P., et al. (2023): Interplay of dopant and polarons in trifunctional semimagnetic semiconductor for supercapacitor applications: Local structure and electronic structure investigations. *Journal of Energy Storage, 60,* 106655. doi: 10.1016/j.est.2023.106655
19. Li R., Zhang C., Liu J., Zhou J., Xu L. (2019): A review on the electrical properties of doped $SrTiO_3$ as anode materials for solid oxide fuel cells. *Materials Research Express, 6*(10), 102006. doi: 10.1088/2053-1591/ab4303
20. Blennow P., Hagen A., Hansen K. K., Wallenberg L. R., Mogensen M. (2008): Defect and electrical transport properties of Nb-doped $SrTiO_3$. *Solid State Ionics, 179*(35-36), 2047-2058. doi: 10.1016/j.ssi.2008.06.023
21. Pan W., Cao M., Hao H., Yao Z., Yu Z., Liu H. (2020): Defect engineering toward the structures and dielectric behaviors of (Nb, Zn) co-doped $SrTiO_3$ ceramics. *Journal of the European Ceramic Society, 40*(1), 49-55. doi: 10.1016/j.jeurceramsoc.2019.09.027
22. Fu Q. Q., Gu H., Xing J. J., Cao Z., Wang J. (2022): Controlling the A-site deficiency and oxygen vacancies by donor-doping in pre-reductive-sintered thermoelectric $SrTiO_3$ ceramics. Acta *Materialia*, *229*, 117785. doi: 10.1016/j.actamat.2022.117785
23. Kobayashi M., Suzuki Y., Goto T., Cho S. H., Sekino T., Asakura Y., Yin S. (2018): Low-temperature hydrothermal synthesis and characterization of $SrTiO_3$ photocatalysts for NOx degradation. *Journal of the Ceramic Society of Japan, 126*(2), 135-138. doi: 10.2109/jcersj2.17195
24. Shannon R. D. (1976): Revised effective ionic radii and systematic studies of interatomic distances in halides and chalcogenides. *Acta crystallographica section A: crystal physics, diffraction, theoretical and general crystallography, 32*(5), 751-767. doi: 10.1107/S0567739476001551
25. Alkathy M. S., Raju K. J. (2018): Enhancement of dielectric properties and energy storage density of bismuth and lithium co-substituted strontium titanate ceramics. *Ceramics International, 44*(9), 10367-10375. doi: 10.1016/j.ceramint.2018.03.049
26. Kassim H., Ibrahim K. E. (2023): Experimental and DFT study on the effect of Mn doping on the structural and optical properties of CuO nanoparticles. *Ceramics–Silikáty, 67*(3), 379-386. doi: 10.13168/cs.2023.0038
27. Azough F., Gholinia A., Alvarez-Ruiz D. T., Duran E., Kepaptsoglou D. M., Eggeman A. S., et al. (2019): Self-nanostructuring in $SrTiO_3$: a novel strategy for enhancement of thermoelectric response in oxides. *ACS applied materials & interfaces, 11*(36), 32833-32843. doi: 10.1021/acsami.9b06483
28. Yadoji P., Peelamedu R., Agrawal D., Roy R. (2003): Microwave sintering of Ni–Zn ferrites: comparison with conventional sintering. *Materials Science and Engineering: B, 98*(3), 269-278. doi: 10.1016/S0921-5107(03)00063-1
29. Zuo F., Carry C., Saunier S., Marinel S., Goeuriot D. (2013): Comparison of the microwave and conventional sintering of alumina: effect of MgO doping and particle size. *Journal of the American Ceramic Society, 96*(6), 1732-1737. doi: 10.1111/jace.12320
30. Chen Y., Fan B., Yang B., Ma W., Liu G., Li H. (2019): Microwave sintering and fracture behaviour of zirconia ceramics. *Ceramics International, 45*(14), 17675-17680. doi: 10.1016/j.ceramint.2019.05.334
31. Farag S., Konyashin I., Ries B. (2018): The influence of grain growth inhibitors on the microstructure and properties of submicron, ultrafine and nano-structured hardmetals – A review. International *Journal of Refractory Metals and Hard Materials, 77*, 12-30. doi: 10.1016/j.ijrmhm.2018.07.003
32. Chen Y. L., Yang S. F. (2011): PTCR effect in donor doped barium titanate: review of compositions, microstructures, processing and properties. *Advances in Applied Ceramics, 110*(5), 257-269. doi: 10.1179/1743676111Y.0000000001
33. Psarras G. C. (2018). Fundamentals of dielectric theories. In *Dielectric Polymer Materials for High-Density Energy Storage* (pp. 11-57). William Andrew Publishing. doi: 10.1016/B978-0-12-813215-9.00002-6
34. Alkathy M. S., Pattipaka S., Gatasheh M. K., Zabotto F. L., Eiras J. A. (2023): Manganese and Magnesium Co-doped Barium Titanate: A Route Towards Enhanced Energy Storage Performance via Defect Dipoles Engineering. *Journal of Inorganic and Organometallic Polymers and Materials*, 1-15. (article in press) doi: 10.1007/s10904-023-02891-7
35. Kossi S. E., Rayssi C., Dhahri A. H., Dhahri J., Khirouni K. (2018): High dielectric constant and relaxor behavior in $La_{0.7}Sr_{0.25}Na_{0.05}Mn_{0.8}Ti_{0.2}O_3$ manganite. *Journal of Alloys and Compounds, 767*, 456-463. doi: 10.1016/j.jallcom.2018.07.056
36. Quan B., Shi W., Ong S. J. H., Lu X., Wang P. L., Ji G., et al. (2019): Defect engineering in two common types of dielectric materials for electromagnetic absorption applications. *Advanced Functional Materials, 29*(28), 1901236. doi: 10.1002/adfm.201901236
37. Morsalin S., Phung T. B., Danikas M., Mawad D. (2019): Diagnostic challenges in dielectric loss assessment and interpretation: a review. *IET Science, Measurement & Technology, 13*(6), 767-782. doi: 10.1049/iet-smt.2018.5597
38. Pang M. C., Marinescu M., Wang H., Offer G. (2021): Mechanical behaviour of inorganic solid-state batteries: can we model the ionic mobility in the electrolyte with Nernst–Einstein's relation? *Physical Chemistry Chemical Physics, 23*(48), 27159-27170. doi: 10.1039/D1CP00909E
39. Huang H., Chen X., Yin K., Treufeld I., Schuele D. E., Ponting M., et al. (2018): Reduction of ionic conduction loss in multilayer dielectric films by immobilizing impurity ions in high glass transition temperature polymer layers. *ACS Applied Energy Materials, 1*(2), 775-782. doi: 10.1021/acsaem.7b00211
40. Jonscher A. K. (1978): Analysis of the alternating current properties of ionic conductors. *Journal of Materials Science, 13*, 553-562. doi: 10.1007/BF00541805
41. Chelidze T. L., Gueguen Y. (1999): Electrical spectroscopy of porous rocks: a review – I. Theoretical models. *Geophysical Journal International, 137*(1), 1-15. doi: 10.1046/j.1365-246x.1999.00799.x
42. Alkathy M. S., Raju K. J. (2016): Effect of Bi and Li co-substituted $SrTiO_3$ ceramics on structural and dielectric properties. *Journal of Materials Science: Materials in Electronics*, *27*, 8957-8965. doi: 10.1007/s10854-016-4926-2
43. Wang Q., Xue X., Lei Y., Wang Y., Feng Y., Xiong X., et al. (2020): Engineering of electronic states on Co_3O_4 ultrathin nanosheets by cation substitution and anion vacancies for oxygen evolution reaction. *Small, 16*(24), 2001571. doi: 10.1002/smll.202001571
44. Li Z., Bosman M., Yang Z., Ren P., Wang L., Cao L., et al. (2012): Interface and surface cation stoichiometry modified

by oxygen vacancies in epitaxial manganite films. *Advanced Functional Materials, 22*(20), 4312-4321. doi: 10.1002/adfm.201200143

45. Nguyen T. L., Dokiya M., Wang S., Tagawa H., Hashimoto T. (2000): The effect of oxygen vacancy on the oxide ion mobility in $LaAlO_3$-based oxides. *Solid State Ionics, 130*(3-4), 229-241. doi: 10.1016/S0167-2738(00)00640-8
46. Presto S., Artini C., Pani M., Carnasciali M. M., Massardo S., Viviani M. (2018): Ionic conductivity and local structural features in $Ce_{1-x}Sm_xO_{2-x}$/2. Physical *Chemistry Chemical Physics, 20*(44), 28338-28345. doi: 10.1039/C8CP04186E
47. Tyunina M. (2020): Oxygen vacancies in perovskite oxide piezoelectrics. Materials, 13(24), 5596. doi: 10.3390/ma13245596
48. Maier J. (1993): Defect chemistry: composition, transport, and reactions in the solid state; part I: thermodynamics. *Angewandte Chemie International Edition in English, 32*(3), 313-335. doi: 10.1002/anie.199303133
49. Nowotny J., Alim M. A., Bak T., Idris M. A., Ionescu M., Prince K., et al. (2015): Defect chemistry and defect engineering of TiO_2-based semiconductors for solar energy conversion. *Chemical Society Reviews, 44*(23), 8424-8442. doi: 10.1039/C4CS00469H
50. Pereira J. S., Guerrero F., Romaguera-Barcelay Y., Anglada-Rivera J., Sales J. C. C., Silva R. S., et al. (2018): $La_{0.59}Li_{0.24}TiO_3$ ceramics obtained by spark plasma sintering: electric behavior analysis. *Materials Research Express, 6*(1), 015504. doi: 10.1088/2053-1591/aae496